PCCP

ROYAL SOCIETY OF CHEMISTRY

PAPER

View Article Online
View Journal | View Issue

Cite this: *Phys. Chem. Chem. Phys.*, 2026, **28**, 3693

Multi-site CO_2 fixation in triazolates: cooperative *O,N* binding enhanced by solvation and counter-ion effects

Puthiyavalappil K. Arathi,[ab] D. Sudha[a] and Cherumuttathu H. Suresh *[abc]

Received 26th November 2025,
Accepted 15th January 2026

DOI: 10.1039/d5cp04586j

rsc.li/pccp

The cooperative interaction of nitrogen and oxygen centers in aromatic heterocycles provides an effective pathway for charge-assisted CO_2 capture. Building on the pioneering work of Luo *et al.* on hydroxy-pyridine systems and our recent PCCP study on hydroxy-substituted N-heterocycles, this work extends the *O,N*-cooperative binding concept to triazolate frameworks. Density functional theory (DFT) and molecular electrostatic potential (MESP) analyses were performed on neutral, monoanionic, and dianionic 1,2,3- and 1,2,4-triazoles to elucidate how charge, counter-ion and solvation govern CO_2 adsorption. Deprotonation generates anionic and dianionic triazolates with enhanced negative potential at N and O sites, enabling *O*-carboxylate and *N*-carboxylate formation. While gas-phase dianions capture multiple CO_2 molecules through cooperative charge delocalization and carbonate-chain growth (up to three CO_2 with $\Delta G_{ad} \approx -54$ kcal mol^{-1}), the inclusion of ethanol solvation and tetramethylphosphonium counter-ions reveals that these species remain strongly exergonic. Reaction modeling shows that both mono- and dianionic triazolates undergo spontaneous CO_2 fixation in solution ($\Delta G \approx 24$ to -61 kcal mol^{-1}), forming ion-paired poly(carboxylate) complexes with up to six CO_2 molecules. These results demonstrate that even under polar, solvated conditions, counter-cation-stabilized triazolates preserve high-affinity, multi-site CO_2 capture, identifying them as realistic and promising building blocks for molecular CO_2-activation strategies.

Introduction

The continuous rise in atmospheric carbon dioxide (CO_2) concentration remains one of the major contributors to global climate change.[1–3] Developing efficient and sustainable CO_2 capture and utilization strategies is therefore a key challenge in modern physical chemistry.[4–6] Among the diverse approaches, molecular and material-based sorbents capable of reversible chemical binding of CO_2 have received increasing attention because of their tunability and potential for low-energy regeneration.[7–9]

Conventional sorbents such as aqueous amines, zeolites, and metal–organic frameworks (MOFs) each have intrinsic limitations.[10–13] Amine scrubbing processes suffer from thermal degradation, volatility, and high regeneration costs, while solid sorbents such as MOFs and zeolites often display reduced uptake under humid or low-partial-pressure conditions.[14–16] These challenges have prompted the design of new molecular adsorbents that exploit charge-assisted, donor–acceptor, and cooperative electrostatic interactions to achieve strong yet reversible CO_2 binding under mild conditions.[17–19]

Hardacre and co-workers demonstrated that a triazole-based superbasic ionic liquid, comprising a phosphonium cation paired with a 1,2,4-triazolate anion, enables efficient electrochemical reduction of CO_2 to formate at remarkably low overpotentials.[20] Another major advance in this direction was reported by Luo *et al.* who demonstrated extraordinarily high CO_2 capacities (up to 1.6 mol CO_2 per mol ionic liquid) in pyridine-containing, anion-functionalized ionic liquids.[14] Their study established that multiple-site cooperative interactions involving simultaneous engagement of oxygen (phenolate) and nitrogen (pyridine) centers with the electrophilic carbon of CO_2 generate synergistic stabilization far exceeding that of single-site binding. Quantum-chemical analysis revealed that π-electron delocalization across the aromatic framework enhances charge transfer to CO_2, while calorimetric data confirmed the thermodynamic feasibility of the process. This discovery provided a conceptual foundation for designing multi-donor anions capable of charge-delocalized, cooperative CO_2 fixation.

Building on this breakthrough, our group recently extended the *O,N*-cooperative binding concept to hydroxy-substituted

[a] *Chemical Sciences and Technology Division, CSIR-National Institute for Interdisciplinary Science and Technology, Thiruvananthapuram, 695019, India. E-mail: sureshch@gmail.com*
[b] *Academy of Scientific and Innovative Research (AcSIR), Ghaziabad, 201002, India*
[c] *Srinivasa Ramanujan Institute for Basic Sciences, Kerala State Council for Science, Technology and Environment, Kottayam, Kerala 686501, India*

aromatic N-heterocycles.[21] DFT calculations showed that hydroxy-pyridine, dihydroxy-naphthyridine, and trihydroxy-pyridonaphthyridine systems exhibit progressively stronger CO_2 adsorption through synergistic *N*,*O* interactions. The adsorption capacity scales with the number of basic and hydroxy sites, enabling one, two, and three CO_2 molecules to associate with the pyridine, naphthyridine, and pyridonaphthyridine frameworks, respectively. Anionic species form covalent-type adducts with CO_2, further stabilized by counter-cations such as Li^+ or $(CH_3)_4P^+$. Solvation slightly weakens the interaction energies but ion-paired systems remain highly exergonic. This work established multi-site, charge-assisted *O*,*N*-binding as a general molecular strategy for designing high-affinity CO_2 adsorbents.

Extending this concept, triazoles—particularly 1,2,3-triazole and 1,2,4-triazole offer a versatile molecular platform for exploring charge-delocalized CO_2 binding. Each triazole ring contains three chemically distinct nitrogen atoms—two pyridine-like and one pyrrole-like—that provide multiple Lewis-basic centers for interaction with CO_2.[22–25] The aromatic and π-excessive nature of triazoles imparts notable electronic flexibility, while hydroxy substitution and subsequent deprotonation generate anionic and dianionic triazolates with negative charge delocalized across N and O atoms. Such frameworks are expected to support cooperative *O*-carboxylate ($-OCO_2^-$) and *N*-carboxylate ($-NCO_2^-$) formation analogous to that in hydroxy-pyridine systems, potentially offering even stronger charge-assisted stabilization through extended conjugation and multi-site coordination.

Despite extensive studies on triazoles in catalysis, coordination chemistry, and energetic materials, their potential as molecular CO_2 capture agents have received little attention.[26,27] The influence of deprotonation, charge delocalization, and solvation on CO_2-binding strength has not been systematically investigated, leaving the underlying electronic principles of triazolate-based CO_2 fixation largely unexplored.

In this work, we present a density functional theory (DFT) investigation of neutral, monoanionic, and dianionic derivatives of 1,2,3- and 1,2,4-triazoles to elucidate how molecular charge, electronic structure, and solvation govern CO_2 adsorption. Molecular electrostatic potential (MESP) analysis is employed to locate reactive sites and visualize charge redistribution upon CO_2 coordination. Solvent and counter-cation effects are modeled using the SMD solvation framework (ethanol) and the tetramethylphosphonium cation, analogous to the phosphonium ionic liquids studied by Luo *et al.* The results reveal a systematic enhancement in CO_2 adsorption energy from neutral to dianionic species, driven by cooperative charge delocalization and orbital overlap. These insights identify triazolate frameworks as promising multi-site, charge-assisted CO_2 capture motifs, extending the *O*,*N*-cooperative mechanism established for hydroxy-pyridine systems to a new class of nitrogen-rich heterocycles. The present work is not intended to model a complete catalytic cycle or bulk-phase CO_2 fixation. Instead, it focuses on establishing intrinsic structure–energy relationships governing CO_2 binding to neutral, anionic, and dianionic triazole-based motifs. This molecular-level approach enables isolation of the fundamental electronic factors controlling CO_2 activation, which would be obscured in fully dynamical or bulk-phase simulations.

Methodology

All density functional theory (DFT) calculations were carried out using the M06-2X hybrid *meta*-GGA functional,[28] which provides a reliable description of noncovalent and charge-assisted interactions. The M06-2X functional is particularly effective for accurately modelling intermolecular non-covalent interactions, which are critical for understanding CO_2–adsorbent complexes.[28] The cc-pVQZ basis set[29] was employed for all geometry optimizations and single-point energy calculations after benchmarking against 6-311++G(d,p), cc-pVDZ, cc-pVTZ, and cc-pV5Z (Table S1). The most extended basis set, cc-pV5Z, produced interaction energies that differ by less than 4% from those obtained using cc-pVQZ. The widely used 6-311++G(d,p) basis set performed reasonably well for many systems, but deviations of up to 18% were observed for some species (Table S1). Therefore, considering both accuracy and computational efficiency, the M06-2X/cc-pVQZ level of theory was adopted for all subsequent calculations. To further validate the robustness of the chosen computational protocol, a benchmark assessment was performed on representative neutral, monoanionic, and dianionic triazole–CO_2 complexes using correlation-consistent basis sets of increasing flexibility, namely aug-cc-pVTZ, and aug-cc-pVQZ, both with and without empirical dispersion corrections (GD3). This analysis was carried out to evaluate the influence of diffuse functions and dispersion on adsorption energetics, which can be particularly relevant for anionic and weakly bound systems. The benchmark results (Table S2) indicate that basis-set augmentation and dispersion inclusion lead only minor structural changes and yield negligible differences in adsorption energies. These findings confirm that the interaction energies are effectively converged at the M06-2X/cc-pVQZ level, justifying its use for the full set of calculations reported in this study. All calculations were performed with Gaussian 16 (revision C.01).[30]

Neutral, monoanionic, and dianionic forms of 1,2,3- and 1,2,4-triazoles were examined along with their hydroxy, deprotonated (anionic), and double-deprotonated (dianionic) derivatives. In this work, the deprotonated species are formally referred to as triazolates; the terms anionic and dianionic triazoles are used for brevity. Geometry optimizations were followed by vibrational-frequency analyses to confirm that all stationary points correspond to minima (no imaginary frequencies). Thermal corrections at 298 K were included in the reported Gibbs free energies.

To eliminate basis set superposition error (BSSE) arising from basis set incompleteness in the weakly bound complexes, all interaction energies were corrected using the Boys–Bernardi counterpoise method.[31] The adsorption energy (ΔE_{ad}) was evaluated as:

$$\Delta E_{ad} = E_{complex} - \left(E_{triazole/triazolate} + E_{CO_2}\right) + E_{BSSE} \quad (1)$$

The corresponding Gibbs free energy of adsorption,

$$\Delta G_{ad} = G_{complex} - (G_{triazole/triazolate} + G_{CO_2}) + E_{BSSE} \quad (2)$$

Molecular electrostatic potential (MESP)[32,33] topographical analysis was performed on all complexes at the M06-2X/cc-pVQZ level to understand intermolecular interactions and electron density delocalization from the molecule to adsorbed CO_2.[34–36] The MESP minimum or the most negative MESP value is observed at electron-rich sites such as π-regions and lone-pair regions. This minimum (V_{min}) is a (3, +3) critical point (CP) in the topography of MESP.[37–39]

Solvent effects[40] were modeled with the SMD (solvation model based on density) within the self-consistent reaction field (SCRF) implicit solvation model[41,42] using ethanol as the representative polar medium. To examine the influence of counterions, the tetramethylphosphonium cation $(CH_3)_4P^+$ was used as a computationally tractable analogue of bulky phosphonium ionic–liquid cations employed experimentally. All solvation calculations were carried out using fully optimized geometries at the M06-2X/SMD/cc-pVQZ level, except for the larger cation–anion paired systems, which were optimized at the M06-2X/SMD/cc-pVTZ level. All structures and energies are provided in the SI.

Results and discussion

Structural and energetic benchmarking

Triazole exists in two structural isomers, 1,2,3-triazole (Tz3) and 1,2,4-triazole (Tz4), each of which can adopt two N–H tautomers depending on the proton position within the ring. This leads to four parent forms, denoted Tz3-1H, Tz3-2H, Tz4-1H, and Tz4-4H. From these, representative mono- and dihydroxy derivatives were generated by substitution at the ring carbon positions, followed by single or double deprotonation to obtain the corresponding monoanionic and dianionic species. The complete set of structures, nomenclature, and substitution patterns considered in this work are summarized in Fig. S1. In the following discussion, emphasis is placed not on individual tautomeric distinctions but on general structure–property relationships, particularly the effects of charge state, substitution, and available donor sites on CO_2 binding behavior. Since the study involves anionic and dianionic species, reliable structural and energetic characterization requires the use of large multiple-ζ basis sets.

Analysis of total electronic energies identified the most stable species within each category (Fig. 1). Among the neutral forms, Tz3-2H (**1**) and Tz4-1H (**2**) are the most stable tautomers. For the hydroxy derivatives, Tz3-2H-4OH ($\mathbf{1_{OH}}$) and Tz4-1H-5OH ($\mathbf{2_{OH}}$) are the lowest-energy forms, while the most stable dihydroxy derivatives are Tz3-2H-4,5OH ($\mathbf{1_{OH2}}$) and Tz4-1H-3,5OH ($\mathbf{2_{OH2}}$). The corresponding monoanions with the lowest energies are Tz3-2H-4O$^-$ ($\mathbf{1_{O-}}$) and Tz4-1H-3O$^-$ ($\mathbf{2_{O-}}$), and the most stable dianions are Tz3-2H-4,5O^{2-} ($\mathbf{1_{O2-}}$) and Tz4-4H-3,5O^{2-} ($\mathbf{2_{O2-}}$). These species were therefore selected for detailed investigation of CO_2-binding interactions.

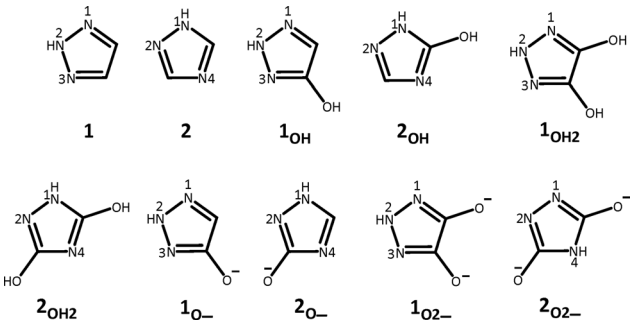

Fig. 1 Neutral, anionic, and dianionic systems considered for CO_2 capture.

MESP analysis of neutral triazole systems and their CO_2 complexes

The MESP topography of representative neutral 1,2,3-triazole systems (Fig. 2) reveals distinct (3, +3) critical points corresponding to the lone-pair regions of nitrogen and oxygen atoms (see Fig. S2 for 1,2,4-triazole systems). These local potential minima (V_{min}) quantitatively describe the electron-rich zones responsible for electrophilic interactions with CO_2. Hydroxy substitution leads to a systematic decrease in electron density at the nitrogen centers, manifested as less negative V_{min} values, indicating reduced basicity and nucleophilicity of these sites.

MESP maps projected on the 0.005 a.u. electron density isosurfaces (Fig. 3) further elucidate the electrostatic complementarity between CO_2 and the triazole ring (see Fig. S3 for 1,2,4-triazole systems). The carbon center of CO_2 exhibits a pronounced electropositive potential (red region), while its oxygens display moderately negative potentials ($V_{min} \approx -13.2$ kcal mol^{-1}). In the $\mathbf{1}\cdots CO_2$ complex, the carbon atom of CO_2 aligns toward the nitrogen lone pair of the triazole, forming a weak N → C interaction that partially transfers electron density to CO_2. This results in a reduction in the negative potential around the interacting nitrogen and a corresponding increase in electron density on the CO_2 oxygen atoms.

Similar patterns of potential redistribution are observed for $\mathbf{1_{OH}}\cdots CO_2$ and $\mathbf{1_{OH2}}\cdots CO_2$ complexes, where the interacting nitrogen exhibits a pronounced decrease in V_{min} upon CO_2 coordination (see Fig. S3 for 1,2,4-triazole systems). In addition, a stabilizing hydrogen bond is often formed between the hydroxy group and the oxygen of CO_2, further reducing the negative potential at the involved oxygen site. Overall, CO_2 complexation leads to a more uniform MESP distribution,

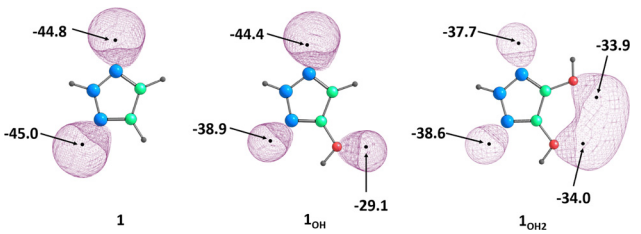

Fig. 2 MESP isosurfaces of **1**, $\mathbf{1_{OH}}$, and $\mathbf{1_{OH2}}$ computed at the M06-2X/cc-pVQZ level of theory. Black dots mark V_{min} positions. Isosurface value: −12.0 kcal mol^{-1}. Color key: gray – H, blue – N, green – C, red – O.

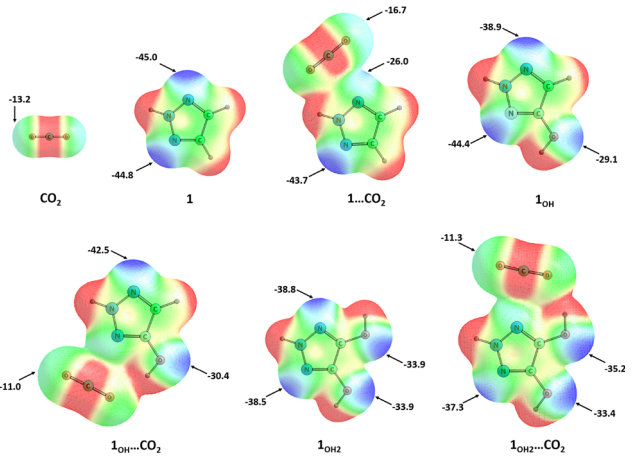

Fig. 3 MESP on the 0.005 a.u. isodensity surface for CO_2, **1**, $\mathbf{1_{OH}}$, $\mathbf{1_{OH2}}$, and their CO_2 complexes. V_{min} values (kcal mol^{-1}) and N···C, O–H···O distances (Å) at the M06-2X/cc-pVQZ level of theory. Color gradient: blue (electron-rich) to red (electron-deficient).

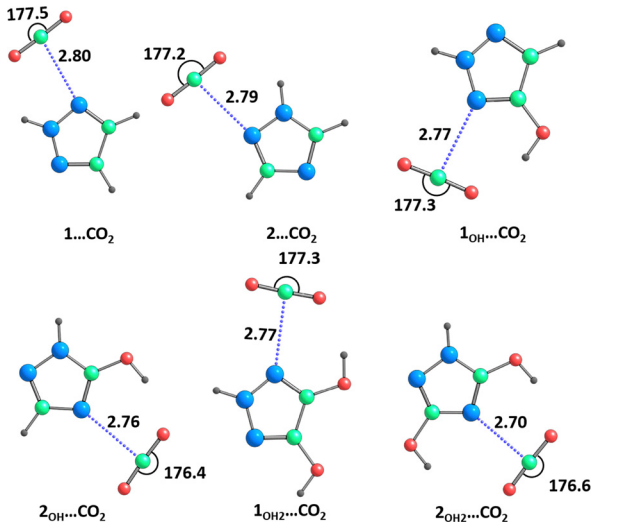

Fig. 4 Optimized geometries of the neutral triazole–CO_2 complexes computed at the M06-2X/cc-pVQZ level of theory. Bond lengths are in Å and bond angles in degrees. Color key: gray – H, blue – N, green – C, red – O.

reflecting enhanced charge delocalization and electrostatic stabilization in the complex.

Structures and interaction energies of triazole–CO_2 complexes

The most stable CO_2 complexes of the neutral triazoles (**1** and **2**), their hydroxy ($\mathbf{1_{OH}}$ and $\mathbf{2_{OH}}$), and dihydroxy ($\mathbf{1_{OH2}}$ and $\mathbf{2_{OH2}}$) derivatives are illustrated in Fig. 4. In all cases, the CO_2 molecule interacts primarily with one of the two nitrogen atoms of the triazole ring through its electrophilic carbon center. The optimized N···C distances lie in the range of 2.75–2.85 Å, accompanied by a slight deviation of the O–C–O angle from linearity (177–179°), indicative of a weak donor–acceptor interaction.

The computed adsorption energies (ΔE_{ad}) for these complexes range from −4.4 to −6.6 kcal mol^{-1}, while the corresponding Gibbs free energies (ΔG_{ad}) are positive, between +2.6 and +3.7 kcal mol^{-1} (Table 1). These values confirm that the interaction of CO_2 with neutral triazole derivatives is thermodynamically unfavorable in the gas phase, consistent with their weakly polar and nonionic nature. Among all studied systems, $\mathbf{2_{OH2}}\cdots CO_2$ exhibits the largest stabilization energy (ΔE_{ad} = −6.6 kcal mol^{-1}), reflecting the cooperative contribution of electron-donating hydroxy groups and possible OH···O hydrogen bonding with CO_2.

Despite these modest binding energies, the presence of substituents such as hydroxy groups significantly enhances the CO_2 affinity of triazoles by locally increasing the electron density around the nitrogen sites and by enabling additional electrostatic or hydrogen-bonding contacts. Overall, the results for the neutral systems establish a baseline for comparison with their anionic and dianionic counterparts, where deprotonation and charge delocalization are expected to greatly strengthen the CO_2 binding interaction.

MESP analysis of CO_2 binding in anionic triazoles

The MESP maps of the anions $\mathbf{1_{O-}}$ and $\mathbf{2_{O-}}$, along with their corresponding CO_2 adducts, are shown in Fig. 5. Compared with their neutral precursors ($\mathbf{1_{OH}}$ and $\mathbf{2_{OH}}$) both anions exhibit

Table 1 BSSE-corrected adsorption energies (ΔE_{ad}) and free energies (ΔG_{ad}) of neutral triazole–CO_2 complexes computed at the M06-2X/cc-pVQZ level of theory (in kcal mol^{-1})

Triazole–CO_2 complex	ΔE_{ad}	ΔG_{ad}
$\mathbf{1}\cdots CO_2$	−4.4	3.6
$\mathbf{2}\cdots CO_2$	−4.8	3.7
$\mathbf{1_{OH}}\cdots CO_2$	−5.2	3.5
$\mathbf{2_{OH}}\cdots CO_2$	−6.4	2.6
$\mathbf{1_{OH2}}\cdots CO_2$	−5.2	3.5
$\mathbf{2_{OH2}}\cdots CO_2$	−6.6	2.7

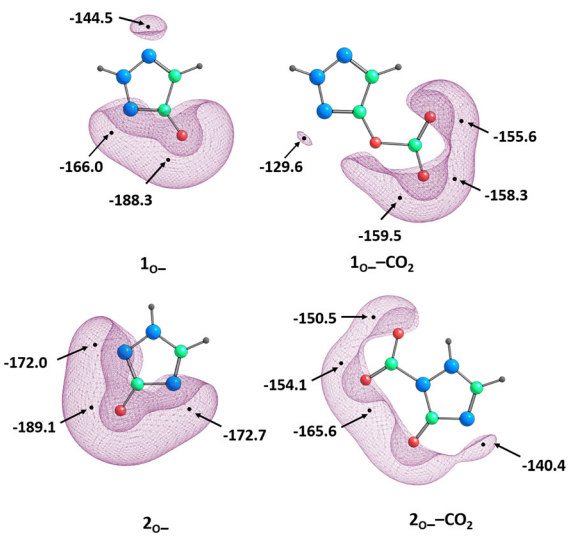

Fig. 5 MESP topography of anions $\mathbf{1_{O-}}$, $\mathbf{2_{O-}}$ and their most stable CO_2 adducts computed at the M06-2X/cc-pVQZ level of theory. Black dots indicate V_{min} value in kcal mol^{-1}. Isosurface value: −125 kcal mol^{-1}. Color key: gray – H, blue – N, green – C, red – O.

substantially more negative electrostatic potentials around the oxygen and nitrogen centers, signifying enhanced nucleophilicity and stronger electrostatic attraction toward the electrophilic carbon of CO_2. The V_{min} values at the oxygen atoms ($V_{min/O}$) are consistently more negative than those at the nitrogen sites ($V_{min/N}$), identifying the O centers as the most favorable sites for CO_2 coordination.

Upon complexation, the most stable CO_2 adduct of $\mathbf{1_{O-}}$ arises when CO_2 binds through its carbon atom to the anionic oxygen site, yielding an *O*-carboxylate species denoted $\mathbf{1_{OCO2-}}$. Among the possible *N*-carboxylate forms involving N_1 and N_3 sites, the N_3-bound adduct ($\mathbf{1_{NCO2-}}$) is the more stable configuration (Table S3 and Fig. S4). For the $\mathbf{2_{O-}}$ anion, however, the preferred adduct is the *N*-carboxylate ($\mathbf{2_{NCO2-}}$) rather than the *O*-bound form ($\mathbf{2_{OCO2-}}$). This reversal of preference suggests that while electrostatic attraction governs the initial approach, the overall stability of the adduct is dictated by charge delocalization and orbital overlap between the N lone pair and the CO_2 antibonding orbitals.

In both *O*- and *N*-carboxylate complexes, significant charge transfer from the anionic triazolate to the CO_2 moiety is reflected by highly negative V_{min} values on the carboxylate oxygens, confirming formation of a delocalized $-OCO_2^-$ fragment. The adsorption of CO_2 on both anions is strongly exothermic ($\Delta E_{ad} \approx -18$ kcal mol^{-1}) and exergonic ($\Delta G_{ad} \approx -6$ kcal mol^{-1}) (Table 2). Between the two systems, $\mathbf{2_{NCO2-}}$ is marginally more stable than $\mathbf{1_{OCO2-}}$, indicating that *N*-centered coordination can be energetically comparable or even superior to *O*-centered binding when favorable orbital interactions operate.

Further adsorption of a second CO_2 molecule on $\mathbf{1_{OCO2-}}$ and $\mathbf{2_{NCO2-}}$ was also explored (Table S4). In both cases, the additional CO_2 interacts noncovalently with the carboxylate group (Fig. 6), producing weakly bound but thermodynamically stable species $\mathbf{1_{OCO2-}}\cdots CO_2$ and $\mathbf{2_{NCO2-}}\cdots CO_2$. Although the second adsorption step is less exothermic ($\approx$10 kcal mol^{-1} stabilization), the overall process remains exergonic by up to 7 kcal mol^{-1}, suggesting that sequential CO_2 capture is feasible. The reduction in binding energy for the second CO_2 is consistent with charge delocalization over the first carboxylate unit, which diminishes localized nucleophilicity.

Interaction of dianionic triazoles with CO_2

The dianionic species $\mathbf{1_{O2-}}$ and $\mathbf{2_{O2-}}$, generated *via* double deprotonation of the dihydroxy derivatives $\mathbf{1_{OH2}}$ and $\mathbf{2_{OH2}}$, exhibit markedly enhanced electron density compared to their monoanionic counterparts. Their MESP maps (Fig. 7) display

Table 2 Adsorption energies (ΔE_{ad}) and Gibbs free energies (ΔG_{ad}) for anionic triazolate–CO_2 adducts at the M06-2X/cc-pVQZ level of theory (kcal mol^{-1})

Anionic systems	ΔE_{ad}	ΔG_{ad}
$\mathbf{1_{OCO2-}}$	−17.8	−5.7
$\mathbf{2_{NCO2-}}$	−18.7	−6.6
$\mathbf{1_{OCO2-}}\cdots CO_2$	−28.0	−7.1
$\mathbf{2_{NCO2-}}\cdots CO_2$	−28.3	−7.3

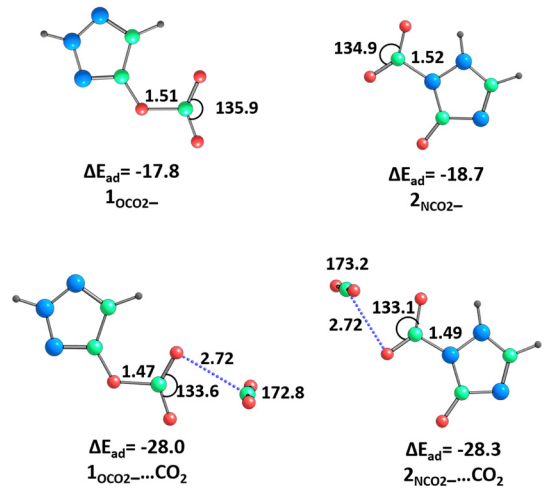

Fig. 6 Optimized geometries of the most stable anionic CO_2 adduct at the M06-2X/cc-pVQZ level of theory. Bond lengths in Å, bond angles in degrees and ΔE_{ad} in kcal mol^{-1}. Color key: gray – H, blue – N, green – C, red – O.

V_{min} values that are approximately 98–99 kcal mol^{-1} more negative than those of the corresponding monoanions, underscoring their exceptional nucleophilic character. Both oxygen and nitrogen centers exhibit high electron density, offering multiple reactive sites for CO_2 binding and thereby increasing the overall CO_2 capture potential.

The first CO_2 adsorption occurs strongly and results in the formation of *N*-carboxylate dianions: $\mathbf{1_{(NCO2-)O-}}$ and $\mathbf{2_{(NCO2-)O-}}$, with adsorption energies (ΔE_{ad}) of −43.9 and −44.0 kcal mol^{-1}, respectively. The corresponding free energies (ΔG_{ad}) of −31.7 and −32.8 kcal mol^{-1} confirm that CO_2 fixation on these dianions is highly exergonic and thermodynamically favorable. These adducts feature short covalent N–C bond distances ($\approx$1.47–1.51 Å), indicative of strong donor–acceptor bonding between the triazolate nitrogen and the carbon center of CO_2.

Subsequent CO_2 adsorption yields distinct bis(carboxylate) complexes depending on the isomer (Table S5). In $\mathbf{1_{(NCO2-)O-}}$, a second CO_2 molecule binds at the remaining N site to form the *N*,*N*′-bis(carboxylate) adduct $\mathbf{1_{(NCO2-)2}}$, while in $\mathbf{2_{(NCO2-)O-}}$, the second CO_2 attaches to the oxygen center, producing an *N*,*O*-bis(carboxylate) complex $\mathbf{2_{(NCO2-)OCO2-}}$. Both species show large cumulative adsorption energies (ΔE_{ad} = −71.9 and

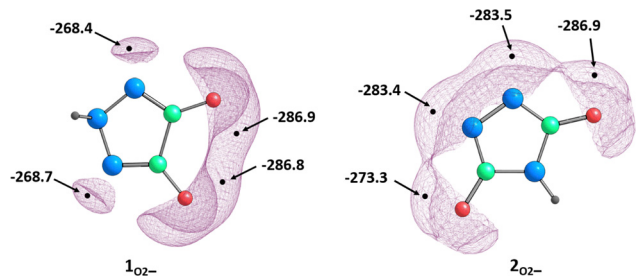

Fig. 7 MESP topography of dianions $\mathbf{1_{O2-}}$ and $\mathbf{2_{O2-}}$ at the M06-2X/cc-pVQZ level of theory. Black dots represent V_{min} positions. Isosurface value: −250 kcal mol^{-1}. Color key: gray – H, blue – N, green – C, red – O.

−73.6 kcal mol^{-1}, respectively), indicating substantial stabilization upon the second CO_2 capture. The incremental binding energies of −28.0 and −29.6 kcal mol^{-1} demonstrate that even after the first CO_2 attachment, additional CO_2 adsorption remains highly favorable.

A third CO_2 molecule can also associate with these bis(carboxylate) dianions. In $\mathbf{1}_{(NCO2-)2}$, the third CO_2 interacts noncovalently with the carboxylate group (O···C ≈ 2.60 Å), giving $\mathbf{1}_{(NCO2-)2}\cdots CO_2$, while in $\mathbf{2}_{(NCO2-)OCO2-}$, the third CO_2 forms a partially covalent O–C bond (1.61 Å), producing $\mathbf{2}_{(NCO2-)(OCO2-)}{-}CO_2$. These tertiary adducts exhibit additional exothermic stabilization (ΔE_{ad} = −85.6 and −87.8 kcal mol^{-1}, respectively), and the corresponding free energies remain negative (ΔG_{ad} ≈ −54 kcal mol^{-1}), demonstrating the thermodynamic viability of sequential CO_2 capture (Table 3 and Fig. 8).

The systematic deepening of the adsorption energy through successive CO_2 additions reflects strong electronic cooperativity within the dianionic framework. Each CO_2 binding event delocalizes charge across multiple carboxylate units, resulting in enhanced electrostatic stabilization and partial activation of the CO_2 molecule-an essential prerequisite for further chemical transformation.

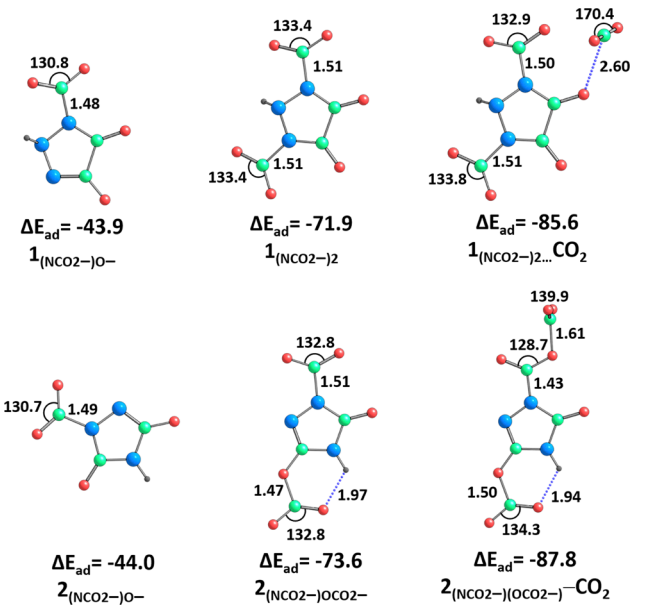

Fig. 8 Optimized structures of CO_2 adduct with dianions at the M06-2X/cc-pVQZ level of theory. Distances in Å, angles in degrees and ΔE_{ad} in kcal mol^{-1}. Color key: gray – H, blue – N, green – C, red – O.

Influence of solvent and counter-cations on CO_2 adsorption

To achieve a realistic description of CO_2 capture behavior, solvent and counter-cation effects were incorporated into the theoretical model. The implicit solvation model (SMD) with ethanol as solvent and the tetramethylphosphonium $(CH_3)_4P^+$ cation as the counter-ion were employed to simulate the experimental environment. This cation, although smaller than bulky trialkylphosphonium analogues, effectively reproduces their electronic characteristics while maintaining computational efficiency.[21]

In ethanol solution, both the *O*-carboxylate $\mathbf{1}_{OCO2-}$ and *N*-carboxylate $\mathbf{2}_{NCO2-}$ exhibit shorter adduct bond distances (without cation) compared with the gas-phase structures (O–C from 1.51 to 1.42 Å and N–C from 1.52 to 1.46 Å) (Fig. 9). These shortened bonds indicate an increase in covalent character within the adducts. Despite this, the adsorption energies in solution ($\Delta E_{ad(s)}$) are reduced by about 5 kcal mol^{-1} relative to gas-phase values due to the stabilizing solvation of the isolated anions. The adsorption process remains exergonic, confirming that CO_2 binding is thermodynamically feasible in solution (Table 4). A second CO_2 molecule binds more weakly through noncovalent interactions, leading to a reduced incremental stabilization.

For the dianionic species, similar patterns are observed. In ethanol, $\mathbf{1}_{(NCO2-)O-}$ and $\mathbf{2}_{(NCO2-)O-}$ exhibit $\Delta E_{ad(s)}$ values of −20.3 and −29.1 kcal mol^{-1}, respectively, corresponding to decreases of 15–24 kcal mol^{-1} relative to the gas-phase data. The bis(carboxylate) adducts $\mathbf{1}_{(NCO2-)2}$ and $\mathbf{2}_{(NCO2-)OCO2-}$ show $\Delta E_{ad(s)}$ = −30.4 and −31.8 kcal mol^{-1}, with respective $\Delta G_{ad(s)}$ = −7.2 and −8.6 kcal mol^{-1}, demonstrating that the complexes remain exergonic even under solvated conditions (Fig. 9). Thus,

Table 3 Adsorption energies (ΔE_{ad}) and Gibbs free energies (ΔG_{ad}) for CO_2 adducts of dianionic triazolates computed at the M06-2X/cc-pVQZ level (kcal mol^{-1})

System	ΔE_{ad}	ΔG_{ad}
$\mathbf{1}_{(NCO2-)O-}$	−43.9	−31.7
$\mathbf{2}_{(NCO2-)O-}$	−44.0	−32.8
$\mathbf{1}_{(NCO2-)2}$	−71.9	−59.1
$\mathbf{2}_{(NCO2-)OCO2-}$	−73.6	−51.1
$\mathbf{1}_{(NCO2-)2}\cdots CO_2$	−85.6	−68.8
$\mathbf{2}_{(NCO2-)(OCO2-)}{-}CO_2$	−87.8	−53.5

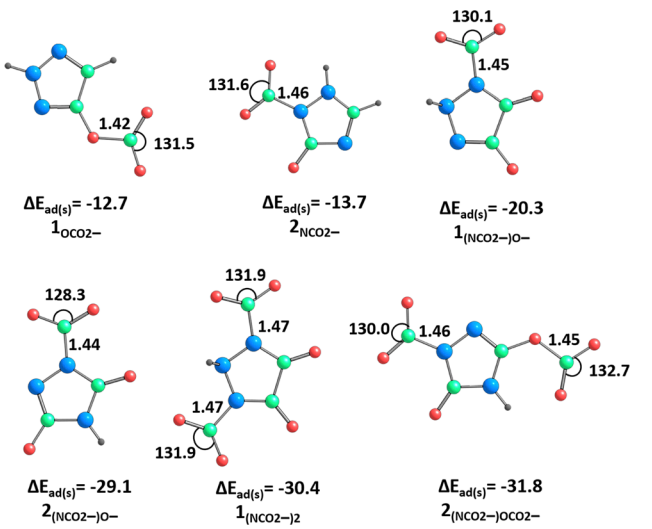

Fig. 9 Optimized geometries of the most stable anionic and dianionic CO_2 adduct in ethanol solvent at the M06-2X/cc-pVQZ level of theory. Bond lengths in Å, bond angles in degrees and ΔE_{ad} in kcal mol^{-1}. Color key: gray – H, blue – N, green – C, red – O.

although solvation weakens the intrinsic adsorption strength, charge delocalization and cooperative binding preserve favorable thermodynamics.

To further elucidate the combined influence of solvation and counter-cations, the energetics of the following solution-phase reactions were examined:

$$(1)\ [\mathbf{1_{OH}}]_{sol} + n[CO_2]_{sol} + [(CH_3)_4P^+(OH^-)]_{sol} \rightarrow [(CH_3)_4P^+(CO_2)\text{-}_{n(\mathbf{1O}-)}]_{sol} + [H_2O]_{sol}$$

$$(2)\ [\mathbf{2_{OH}}]_{sol} + n[CO_2]_{sol} + [(CH_3)_4P^+(OH^-)]_{sol} \rightarrow [(CH_3)_4P^+(CO_2)\text{-}_{n(\mathbf{2O}-)}]_{sol} + [H_2O]_{sol}$$

$$(3)\ [\mathbf{1_{OH2}}]_{sol} + n[CO_2]_{sol} + [2(CH_3)_4P^+(OH^-)]_{sol} \rightarrow [((CH_3)_4P^+)_2(CO_2)_n(\mathbf{1_{O2}}-)]_{sol} + 2[H_2O]_{sol}$$

$$(4)\ [\mathbf{2_{OH2}}]_{sol} + n[CO_2]_{sol} + [2(CH_3)_4P^+(OH^-)]_{sol} \rightarrow [((CH_3)_4P^+)_2(CO_2)_n(\mathbf{2_{O2}}-)]_{sol} + 2[H_2O]_{sol}$$

These reactions describe the interaction of hydroxy-substituted triazoles with phosphonium hydroxide in the presence of CO_2 in solution (sol), leading to the formation of the corresponding anionic or dianionic CO_2 adducts accompanied by the elimination of water. The computed reaction energetics, summarized in Table 5, cover the formation of both anionic complexes (n = 1–3) and dianionic complexes (n = 1–6), providing insight into the stability and CO_2-binding capability of these species in solution.

Table 4 BSSE-corrected adsorption energies ($\Delta E_{ad(s)}$) and Gibbs free energies ($\Delta G_{ad(s)}$) of selected anionic and dianionic triazolate–CO_2 complexes in ethanol solution computed at the M06-2X/SMD/cc-pVQZ level (kcal mol^{-1})

System	$\Delta E_{ad(s)}$	$\Delta G_{ad(s)}$
$\mathbf{1_{OCO2}}-$	−12.7	0.1
$\mathbf{2_{NCO2}}-$	−13.7	−2.0
$\mathbf{1_{(NCO2-)O}}-$	−20.3	−8.6
$\mathbf{2_{(NCO2-)O}}-$	−29.1	−17.7
$\mathbf{1_{(NCO2-)2}}$	−30.4	−7.2
$\mathbf{2_{(NCO2-)OCO2}}-$	−31.8	−8.6

The formation of the anionic complexes is both exothermic and exergonic for n = 1 and n = 2, but becomes endergonic at n = 3 (Table 5). The dianionic complexes exhibit an even stronger thermodynamic driving force: for $\mathbf{1_{O2}}-$, CO_2 addition remains exothermic and exergonic up to n = 4, with the reaction becoming endergonic only upon adsorption of the fifth CO_2 molecule. In comparison, CO_2 binding to $\mathbf{2_{O2}}-$ is even more favorable, showing consistently higher exothermic and exergonic character, and the onset of endergonicity appears only at the adsorption of the seventh CO_2 molecule.

It is noteworthy that for the monoanionic species $\mathbf{1_O}-$, the first CO_2 molecule forms an *O*-carboxylate adduct, whereas for $\mathbf{2_O}-$, the initial binding results in an *N*-carboxylate structure. Subsequent CO_2 molecules are sequentially adsorbed, with the second attaching to the first and the third attaching to the second, giving rise to an extended ''carbonate-chain'' motif (Fig. 10). This chain-like arrangement enables delocalization of the negative charge along the connected CO_2 units. A similar carbonate-chain topology is observed for the dianionic systems $\mathbf{1_{O2}}-$ and $\mathbf{2_{O2}}-$ (Fig. 10). In $\mathbf{1_{O2}}-$, the chain grows outward from an initial *N*-carboxylate site, with additional CO_2 molecules forming a continuous, connected framework. In contrast, in $\mathbf{2_{O2}}-$, the two arms of the dianion extend differently: one side develops through an *N*-carboxylate linkage, while the other propagates *via* an *O*-carboxylate linkage.

These results demonstrate that even in polar solvents, charge-assisted and counter-cation-stabilized binding modes maintain strong thermodynamic favorability. The synergy between solvation, ion pairing, and electronic delocalization underscores the potential of triazolate-based ionic systems for practical CO_2 fixation and activation.

Conclusions

This comprehensive DFT investigation elucidates the structural, electrostatic, and thermodynamic factors governing CO_2 adsorption on 1,2,3- and 1,2,4-triazole derivatives in their neutral, monoanionic, and dianionic forms. Benchmark calculations confirmed that M06-2X/cc-pVQZ provides reliable

Table 5 Reaction energies ($\Delta E_{rea(s)}$) and free energies ($\Delta G_{rea(s)}$) for CO_2 capture by hydroxy and dihydroxy triazoles in ethanol in the presence of $(CH_3)_4P^+(OH)$, computed at the M06-2X/SMD/cc-pVTZ level (kcal mol^{-1})

No.	Reactions in ethanol	$\Delta E_{rea(s)}$	$\Delta G_{rea(s)}$
1	$\mathbf{1_{OH}} + CO_2 + (CH_3)_4P^+(OH)^- \rightarrow (CH_3)_4P^+(CO_2)_1(\mathbf{1_O}-) + H_2O$	−36.0	−23.6
2	$\mathbf{1_{OH}} + 2CO_2 + (CH_3)_4P^+(OH)^- \rightarrow (CH_3)_4P^+(CO_2)_2(\mathbf{1_O}-) + H_2O$	−34.4	−10.5
3	$\mathbf{1_{OH}} + 3CO_2 + (CH_3)_4P^+(OH)^- \rightarrow (CH_3)_4P^+(CO_2)_3(\mathbf{1_O}-) + H_2O$	−25.5	9.0
4	$\mathbf{2_{OH}} + CO_2 + (CH_3)_4P^+(OH)^- \rightarrow (CH_3)_4P^+(CO_2)_1(\mathbf{2_O}-) + H_2O$	−38.0	−25.5
5	$\mathbf{2_{OH}} + 2CO_2 + (CH_3)_4P^+(OH)^- \rightarrow (CH_3)_4P^+(CO_2)_2(\mathbf{2_O}-) + H_2O$	−33.7	−10.3
6	$\mathbf{2_{OH}} + 3CO_2 + (CH_3)_4P^+(OH)^- \rightarrow (CH_3)_4P^+(CO_2)_3(\mathbf{2_O}-) + H_2O$	−25.2	9.1
7	$\mathbf{1_{OH2}} + 2CO_2 + 2\,(CH_3)_4P^+(OH)^- \rightarrow ((CH_3)_4P^+)_2(CO_2)_2(\mathbf{1_{O2}}-) + 2H_2O$	−78.2	−49.4
8	$\mathbf{1_{OH2}} + 3CO_2 + 2\,(CH_3)_4P^+(OH)^- \rightarrow ((CH_3)_4P^+)_2(CO_2)_3(\mathbf{1_{O2}}-) + 2H_2O$	−72.5	−33.0
9	$\mathbf{1_{OH2}} + 4CO_2 + 2\,(CH_3)_4P^+(OH)^- \rightarrow ((CH_3)_4P^+)_2(CO_2)_4(\mathbf{1_{O2}}-) + 2H_2O$	−67.1	−17.0
10	$\mathbf{1_{OH2}} + 5CO_2 + 2\,(CH_3)_4P^+(OH)^- \rightarrow ((CH_3)_4P^+)_2(CO_2)_5(\mathbf{1_{O2}}-) + 2H_2O$	−56.6	2.9
11	$\mathbf{2_{OH2}} + 2CO_2 + 2\,(CH_3)_4P^+(OH)^- \rightarrow ((CH_3)_4P^+)_2(CO_2)_2(\mathbf{2_{O2}}-) + 2H_2O$	−86.7	−61.0
12	$\mathbf{2_{OH2}} + 3CO_2 + 2\,(CH_3)_4P^+(OH)^- \rightarrow ((CH_3)_4P^+)_2(CO_2)_3(\mathbf{2_{O2}}-) + 2H_2O$	−86.7	−49.4
13	$\mathbf{2_{OH2}} + 4CO_2 + 2\,(CH_3)_4P^+(OH)^- \rightarrow ((CH_3)_4P^+)_2(CO_2)_4(\mathbf{2_{O2}}-) + 2H_2O$	−80.1	−31.1
14	$\mathbf{2_{OH2}} + 5CO_2 + 2\,(CH_3)_4P^+(OH)^- \rightarrow ((CH_3)_4P^+)_2(CO_2)_5(\mathbf{2_{O2}}-) + 2H_2O$	−85.4	−27.0
15	$\mathbf{2_{OH2}} + 6CO_2 + 2\,(CH_3)_4P^+(OH)^- \rightarrow ((CH_3)_4P^+)_2(CO_2)_6(\mathbf{2_{O2}}-) + 2H_2O$	−79.9	−10.0

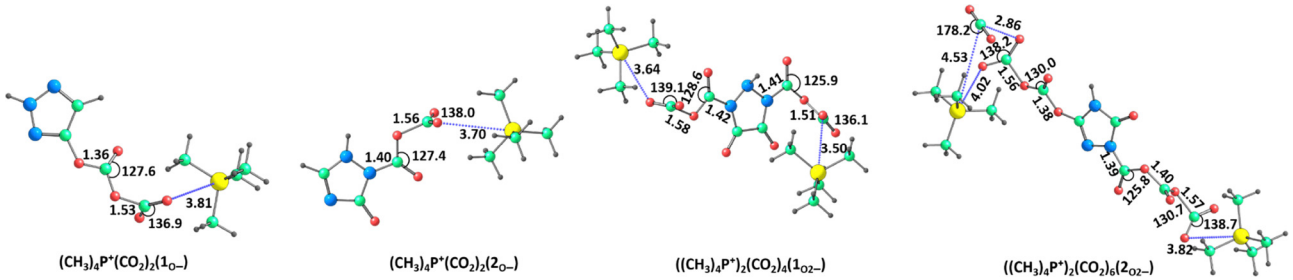

Fig. 10 Representative structures of triazolate–CO_2 adducts in ethanol with tetramethylphosphonium counter-ions, computed at the M06-2X/SMD/cc-pVTZ level. Distances in Å, angles in degrees; Color key: gray – H, blue – N, green – C, red – O, yellow – P.

interaction energies across the series. Molecular electrostatic potential (MESP) analyses established that CO_2 binds preferentially to electron-rich N and O sites, with deprotonation greatly enhancing nucleophilicity and charge-assisted stabilization.

Neutral triazoles exhibit only weak physisorption of CO_2 ($\Delta E_{ad} \approx -4$ to -7 kcal mol^{-1}), while the corresponding anions form strong covalent *O*-carboxylate (–OCO_2^-) and *N*-carboxylate (–NCO_2^-) adducts, releasing 17–19 kcal mol^{-1} of binding energy and showing exergonic adsorption. Successive CO_2 binding on these anions remains energetically favorable through secondary noncovalent interactions. In the dianions, sequential adsorption yields bis(carboxylate) and tris(carboxylate) complexes with stepwise adsorption energies up to -88 kcal mol^{-1}, demonstrating the cooperative electronic effects of multiple charge centers and extensive delocalization.

Crucially, the inclusion of solvation (ethanol) and tetramethylphosphonium counter-cations provides a realistic assessment of CO_2 capture under experimental conditions. Although solvation reduces intrinsic binding strengths, both anionic and dianionic triazolates retain strongly exergonic CO_2 fixation. Solution-phase reaction modeling reveals spontaneous formation of mono- and poly(carboxylate) complexes, with dianions capable of exergonically binding up to six CO_2 molecules. The counter-cation plays a decisive stabilizing role by dispersing charge, modulating local electrostatics, and enabling cooperative adsorption sequences.

Thus, triazolate-based ionic systems combine multi-site *O*,*N* cooperativity, charge-delocalized activation, and counter-ion stabilization to deliver robust CO_2 capture even in polar media. These features position triazolates as promising molecular platforms for realistic CO_2 fixation, activation, and potential downstream conversion.

Author contributions

CHS conceptualized the project, supervised the work, and contributed to the writing of the manuscript. PKA and DS conducted research, curated the data, and contributed to the writing of the manuscript.

Conflicts of interest

There are no conflicts to declare.

Data availability

The data underlying this study are available in the published article and its supplementary information (SI). Supplementary information: SCF energies, zero-point correction, thermal correction to Gibbs free energies and BSSE correction (Table S6) and Cartesian coordinates of all the systems (Table S7). See DOI: https://doi.org/10.1039/d5cp04586j.

Acknowledgements

PKA is thankful to DST, Inspire, for a Senior Research Fellowship. CHS acknowledges CSIR-NIIST, Trivandrum for his deputation assignment as Director to SRIBS, Kottayam.

References

1 F. Pulido and P. Berthold, *Adv. Ecol. Res.*, 2004, **35**, 151–183.
2 K. Caldeira and J. F. Kasting, *Nature*, 1993, **366**, 251–253.
3 D. A. Lashof and D. R. Ahuja, *Nature*, 1990, **344**, 529–531.
4 D. M. D'Alessandro, B. Smit and J. R. Long, *Angew. Chem., Int. Ed.*, 2010, **49**, 6058–6082.
5 J. M. Nordbotten and M. A. Celia, *Geological storage of CO_2: modeling approaches for large-scale simulation, New Jersey, 2011.*
6 J. D. Figueroa, T. Fout, S. Plasynski, H. McIlvried and R. D. Srivastava, *Int. J. Greenhouse Gas Control*, 2008, **2**, 9–20.
7 C. Dhoke, A. Zaabout, S. Cloete and S. Amini, *Ind. Eng. Chem. Res.*, 2021, **60**, 3779–3798.
8 J. Yu, L.-H. Xie, J.-R. Li, Y. Ma, J. M. Seminario and P. B. Balbuena, *Chem. Rev.*, 2017, **117**, 9674–9754.
9 P. Nugent, Y. Belmabkhout, S. D. Burd, A. J. Cairns, R. Luebke, K. Forrest, T. Pham, S. Ma, B. Space and L. Wojtas, *Nature*, 2013, **495**, 80–84.
10 R. Poloni, B. Smit and J. B. Neaton, *J. Am. Chem. Soc.*, 2012, **134**, 6714–6719.
11 L. Du, Z. Lu, K. Zheng, J. Wang, X. Zheng, Y. Pan, X. You and J. Bai, *J. Am. Chem. Soc.*, 2013, **135**, 562–565.
12 J. A. Thompson, N. A. Brunelli, R. P. Lively, J. Johnson, C. W. Jones and S. Nair, *J. Phys. Chem. C*, 2013, **117**, 8198–8207.
13 R. Babarao, R. Custelcean, B. P. Hay and D.-E. Jiang, *Cryst. Growth Des.*, 2012, **12**, 5349–5356.

14 X. Luo, Y. Guo, F. Ding, H. Zhao, G. Cui, H. Li and C. Wang, *Angew. Chem.*, 2014, **126**, 7173–7177.
15 I. Niedermaier, M. Bahlmann, C. Papp, C. Kolbeck, W. Wei, S. Krick Calderon, M. Grabau, P. S. Schulz, P. Wasserscheid and H.-P. Steinrück, *J. Am. Chem. Soc.*, 2014, **136**, 436–441.
16 S. Wang, W.-C. Li, L. Zhang, Z.-Y. Jin and A.-H. Lu, *J. Mater. Chem. A*, 2014, **2**, 4406–4412.
17 H. Tang and C. Wu, *ChemSusChem*, 2013, **6**, 1050–1056.
18 H. M. Lee, I. S. Youn, M. Saleh, J. W. Lee and K. S. Kim, *Phys. Chem. Chem. Phys.*, 2015, **17**, 10925–10933.
19 M. Juríček, P. H. Kouwer and A. E. Rowan, *Chem. Commun.*, 2011, **47**, 8740–8749.
20 N. Hollingsworth, S. R. Taylor, M. T. Galante, J. Jacquemin, C. Longo, K. B. Holt, N. H. De Leeuw and C. Hardacre, *Angew. Chem., Int. Ed.*, 2015, **54**, 14164–14168.
21 P. K. Arathi and C. H. Suresh, *Phys. Chem. Chem. Phys.*, 2025, **27**, 14630–14644.
22 W. Li, X. Zhao, F. Liu and B. Hou, *Corros. Sci.*, 2008, **50**, 3261–3266.
23 V. P. Krivopalov and O. P. Shkurko, *Russ. Chem. Rev.*, 2005, **74**, 339.
24 R. Kharb, P. C. Sharma and M. S. Yar, *J. Enzyme Inhib. Med. Chem.*, 2011, **26**, 1–21.
25 Y. Naito, F. Akahoshi, S. Takeda, T. Okada, M. Kajii, H. Nishimura, M. Sugiura, C. Fukaya and Y. Kagitani, *J. Med. Chem.*, 1996, **39**, 3019–3029.
26 V. V. Chaban and N. A. Andreeva, *J. Mol. Liq.*, 2023, **378**, 121623.
27 R. Boulmène, M. Prakash and M. Hochlaf, *Phys. Chem. Chem. Phys.*, 2016, **18**, 29709–29720.
28 Y. Zhao and D. G. Truhlar, *Theor. Chem. Acc.*, 2008, **120**, 215–241.
29 T. H. Dunning Jr, *J. Chem. Phys.*, 1989, **90**, 1007–1023.
30 M. J. Frisch, G. W. Trucks, H. B. Schlegel, G. E. Scuseria, M. A. Robb, J. R. Cheeseman, G. GScalmani, V. Barone, G. A. Petersson, H. Nakatsuji, X. Li, M. Caricato, A. V. Marenich, J. Bloino, B. G. Janesko, R. Gomperts, B. Mennucci, H. P. Hratchian, J. V. Ortiz, A. F. Izmaylov, J. L. Sonnenberg, D. Williams-Young, F. Ding, F. Lipparini, F. Egidi, J. Goings, B. Peng, A. Petrone, T. Henderson, D. Ranasinghe, V. G. Zakrzewski, J. Gao, N. Rega, G. Zheng, W. Liang, M. Hada, M. Ehara, K. Toyota, R. Fukuda, J. Hasegawa, M. Ishida, T. Nakajima, Y. Honda, O. Kitao, H. Nakai, T. Vreven, K. Throssell, J. A. Montgomery, J. E. Peralta, F. Ogliaro, M. J. Bearpark, J. J. Heyd, E. N. Brothers, K. N. Kudin, V. N. Staroverov, T. A. Keith, R. Kobayashi, J. Normand, K. Raghavachari, A. P. Rendell, J. C. Burant, S. S. Iyengar, J. Tomasi, M. Cossi, J. M. Millam, M. Klene, C. Adamo, R. Cammi, J. W. Ochterski, R. L. Martin, K. Morokuma, O. Farkas, J. B. Foresman and D. J. Fox, *Gaussian 16, Revision A.03*, Gaussian, Wallingford, CT, 2016.
31 S. F. Boys and F. Bernardi, *Mol. Phys.*, 1970, **19**, 553–566.
32 P. Politzer and D. G. Truhlar, *Chemical applications of atomic and molecular electrostatic potentials: reactivity, structure, scattering, and energetics of organic, inorganic, and biological systems*, Boston, 2013.
33 S. R. Gadre and R. N. Shirsat, *Electrostatics of atoms and molecules*, Hyderabad, 2000.
34 N. Mohan and C. H. Suresh, *J. Phys. Chem. A*, 2014, **118**, 1697–1705.
35 P. V. Bijina and C. H. Suresh, *J. Chem. Sci.*, 2016, **128**, 1677–1686.
36 C. H. Suresh and S. Anila, *Acc. Chem. Res.*, 2023, **56**, 1884–1895.
37 C. Suresh and S. R. Gadre, *J. Am. Chem. Soc.*, 1998, **120**, 7049–7055.
38 S. R. Gadre and P. K. Bhadane, *J. Phys. Chem. A*, 1999, **103**, 3512–3517.
39 F. B. Sayyed and C. H. Suresh, *J. Phys. Chem. A*, 2012, **116**, 5723–5732.
40 C. Reichardt, *Org. Process Res. Dev.*, 2007, **11**, 105–113.
41 A. J. Reynolds, T. V. Verheyen, S. B. Adeloju, E. Meuleman and P. Feron, *Environ. Sci. Technol.*, 2012, **46**, 3643–3654.
42 A. V. Marenich, C. J. Cramer and D. G. Truhlar, *J. Phys. Chem. B*, 2009, **113**, 6378–6396.